# CHAPTER 7

# CORROSION BEHAVIOUR

In this chapter, the corrosion behaviour of the indigenously developed bainitic steels and pearlitic steels of the same compositions is discussed. The details are described under sub topics of electrochemical corrosion, immersion corrosion, morphology and EDS analysis of corrosion products, XPS analysis of oxides (corrosion products) and the mechanisms of corrosion. In order to examine the effect of austempering time on the corrosion behaviour of austempered steel and their comparison with patented steel, the electrochemical (potentiodynamic polarization test and electrochemical impedance spectroscopy (EIS)) and immersion test were performed.

## 7.1 ELECTROCHEMICAL CORROSION

### 7.1.1 Potentiodynamic Polarization Test

Figure 7.1 depicts the Tafel plots of bainitic and pearlitic steels. Several electrochemical characteristics, including corrosion current density ($i_{corr}$, $\mu A/cm^2$), corrosion potential ($E_{corr}$, mV), anodic slope ($\beta_a$), cathodic slope ($\beta_c$), and corrosion rate (mm/y), are derived from the Tafel plot and listed in Table 7.1. The Tafel plot for samples B12VA-1, B12VA-2, and P12VA is depicted in Figure 7.1a. $E_{corr}$ of B12VA-1 and P12VA changes toward positive potential with respect to open circuit potential (OCP), except for B12VA-2, which shifts toward the active side; nevertheless, B12VA-2 displays the lowest $i_{corr}$ value. The $E_{corr}$ of B14VA-1 and B14VA-2 likewise changes toward the noble side with regard to OCP, with the exception of P14VA. B14VA-2 sample displays the minimal corrosion current density (Figure 7.1b). Similarly, in Figure 7.1c, $E_{corr}$ of B15VA-1, B15VA-2, and P15VA move toward the positive potential side against OCP, and sample B15VA-2 has the lowest $i_{corr}$ value among the investigated steels (Table 7.1).

Tafel plots reveal the combination of activation and concentration reduction process ($O_2 + 2H_2O + 4e^- = 4OH^-$). Consequently, the Tafel extrapolation technique is used to calculate $i_{corr}$ value. Equation (2.9) is utilized to compute the corrosion rates. B15VA-2 has the lowest corrosion rate of 0.012±0.001mm/year among all the studied steels (Table 7.1). Except for the B14VA-1 sample, bainitic steels have more corrosion resistance than pearlitic steels.

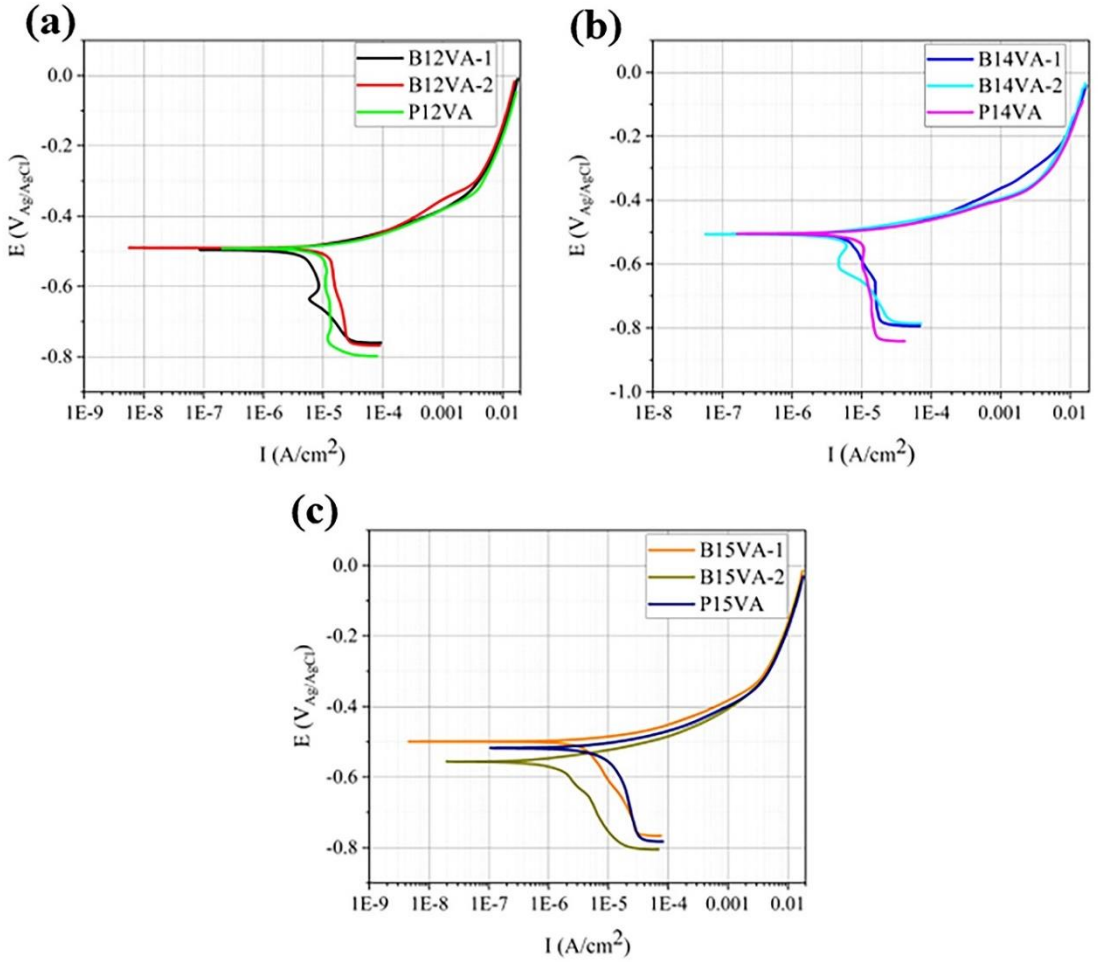


**Figure 7.1** Electrochemical potentiodynamic polarization curves (Tafel plots) of the bainitic and pearlitic steel samples (a) B12VA alloy: B12VA-1, B12VA-2 and P12VA, (b) B14VA alloy: B14VA-1, B14VA-2 and P14VA, and (c) B15VA alloy: B15VA-1, B15VA-2 and P15VA.

$R_p$ may also be determined from a Tafel polarization curve by fitting Tafel data in the potential range of ±20 mV with $R_p$ fitting using the CS studio 5 program; the resulting values are shown in Table 7.1. The maximal $R_p$ value of the sample B15VA-2 is 3029.3 **Ω**/cm$^2$. $R_p$ is directly associated to corrosion resistance and provides crucial information on the reactivity of steels exposed to an aqueous 3.5 wt.% NaCl solution.

**Table 7.1** Electrochemical potentiodynamic polarization parameter, resistance potential ($R_p$) and corrosion rate (CR) of the austempered bainitic steel and patented pearlitic steel.

| Samples | OCP (mV) | $\beta_a$ (mV) | $\beta_c$ (mV) | $I_{corr}$ (μA/cm$^2$) | $E_{corr}$ (V) | $R_p$ (Ω/cm$^2$) | CR (mm/year) |
|---|---|---|---|---|---|---|---|
| B12VA-1 | -515.3 | 37.3 | 624.6 | 5.73 | -0.496 | 2351.8 | 0.056±0.001 |
| B12VA-2 | -522.1 | 42.9 | 97.9 | 1.45 | -0.585 | 2705.2 | 0.014±0.002 |
| P12VA | -536.4 | 44.3 | 949.4 | 12.30 | -0.494 | 1381.2 | 0.120±0.003 |
| B14VA-1 | -548.9 | 37.8 | 834.5 | 9.57 | -0.506 | 1654.7 | 0.094±0.002 |
| B14VA-2 | -541.6 | 47.0 | 370.9 | 6.94 | -0.506 | 1868.5 | 0.068±0.003 |
| P14VA | -500.1 | 49.2 | 136.9 | 16.27 | -0.505 | 1027.3 | 0.159±0.002 |
| B15VA-1 | -522.1 | 27.7 | 266 | 3.86 | -0.499 | 2589.4 | 0.038±0.002 |
| B15VA-2 | -560.7 | 37.9 | 175.3 | 1.25 | -0.556 | 3029.3 | 0.012±0.001 |
| P15VA | -538.4 | 42.8 | 294.1 | 7.85 | -0.517 | 1820.2 | 0.077±0.003 |

### 7.1.2 Electrochemical Impedance Spectroscopy (EIS) Test

Figure 7.2((a), (b) and (c)) depict the Nyquist, Bode magnitude, and Bode phase graphs, respectively derived from EIS test of the studied steels. Figure 7.2 (d) displays a fitted electrical circuit ($R_s$ (CPE $R_{ct}$)), which is used to fit the EIS data in order to obtain the quantitative information of solution resistance ($R_s$), constant phase element (CPE) and $R_{ct}$ (Table 7.2). For the excellent fitting of the EIS data, a Chi-square ($\chi^2$) value of $10^{-3}$ has been favoured. The Nyquist plots (Figure 7.2(a)) of all the studied steels display the indented semicircle, which suggest the occurrence of a single time constant, and the

semicircle is centred on the real axis and demonstrates the frequency dispersion capacitive response [123].

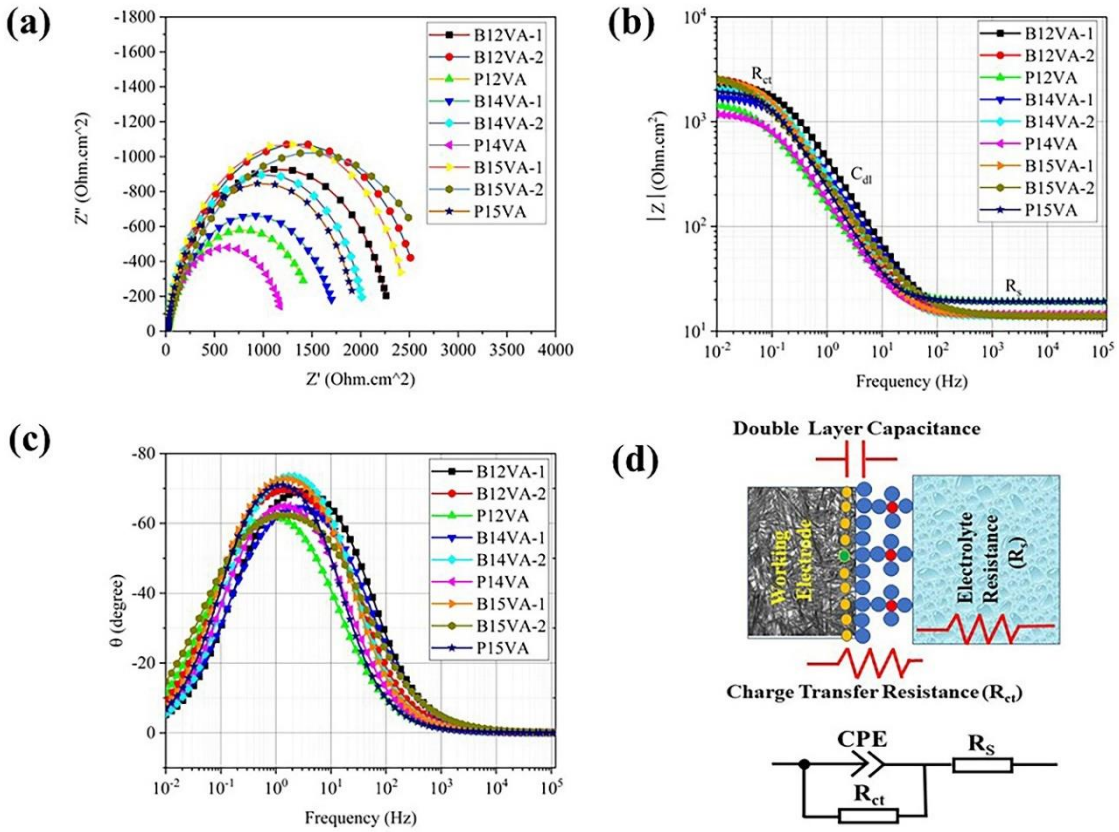


**Figure 7.2** Electrochemical impedance spectroscopy (EIS) plot of the austempered bainitic steel and pearlitic steel: (a) Nyquist plots, (b) Bode magnitude plots, (c) Bode phase plots, and (d) Fitted equivalent electrical circuit and its graphical representation.

$R_{ct}$ is shown by the diameter of the Nyquist plot. Except for the B14VA-1 sample, bainitic steels have a greater $R_{ct}$ than pearlitic steels (Table 7.2). Among the studied steels, sample B15VA-2 has the highest $R_{ct}$ value of 2939.52 $\Omega/cm^2$. Figure 7.2(b) displays Bode magnitude plot. The value of the $R_{ct}$ is represented in the segment of the horizontal section of the Bode magnitude graphs that has the lowest frequency, while the value of the $R_s$ is shown in the region of the Bode magnitude graph that has the greatest frequency. However, the electrical double layer capacitance that develops at the interface of electrode and electrolyte after two hours of OCP stabilization testing in an aqueous

3.5% weight NaCl is the dominant factor in the midfrequency region. All electrochemical measurements utilize the same electrolyte. Therefore, the values of Rs determined from Bode magnitude curves are essentially comparable for all tested steels (Table 7.2). After implementing the most precise RCR circuit, $R_s$ have been determined. The value of $R_s$ is almost similar for the studied steels except for P12VA and P15VA samples, whose values have fluctuated between ±4 Ω/cm$^2$. The $R_{ct}$ value increased in bainitic steel samples with an increase in the Aus. time due to a lower content of RA, and pearlitic steels have the lowest $R_{ct}$ values.

**Table 7.2** Parameters of the electrochemical impedance spectroscopy (EIS) of the austempered and patented steels.

| **Samples** | **$R_s$ (Ω/cm$^2$)** | **CPE ($\Omega^{-1}$ s$^n$ cm$^{-2}$)** | **n** | **$R_{ct}$ (Ω/cm$^2$)** | **$\chi 2$** |
|---|---|---|---|---|---|
| B12VA-1 | 13.95 | 4.47 x10$^{-4}$ | 0.86 | 2308.7±11 | 9.2x10$^{-4}$ |
| B12VA-2 | 13.97 | 6.32 x10$^{-4}$ | 0.86 | 2665.7±13 | 1.37x10$^{-3}$ |
| P12VA | 18.06 | 14.29 x10$^{-4}$ | 0.82 | 1550.2±25 | 6.4x10$^{-4}$ |
| B14VA-1 | 13.95 | 6.4 x10$^{-4}$ | 0.82 | 1760.3±34 | 7.34x10$^{-4}$ |
| B14VA-2 | 13.98 | 6.2 x10$^{-4}$ | 0.92 | 2037.8±24 | 8.64x10$^{-4}$ |
| P14VA | 14.5 | 11.5 x10$^{-4}$ | 0.85 | 1211.7±27 | 5.94x10$^{-4}$ |
| B15VA-1 | 14.19 | 7 x10$^{-4}$ | 0.90 | 2500.4±17 | 1.154x10$^{-3}$ |
| B15VA-2 | 13.86 | 8.9 x10$^{-4}$ | 0.89 | 2939.5±22 | 1.854x10$^{-3}$ |
| P15VA | 18.17 | 8.0 x10$^{-4}$ | 0.91 | 1950.5±19 | 6.64x10$^{-4}$ |

Similarly, the phase angle is greatest in the mid-frequency area of the Bode phase plots (Figure 7.2(c)) and decreases at both the lowest and highest frequency regions. Due to the occurrence of a single maximum in the Bode phase plot, bainitic and pearlitic steel specimens consist of a single time constant. All bainitic steel specimens reveal a wider mid-frequency zone and it is moved towards the lesser frequency spectrum and attempts

to reach its maximum near capacitive region. The CPE of the EDL cannot signify the capacitance when n is less than one at the studied steel electrode/electrolyte boundary.

### 7.1.3 Morphology of Corrosion Products After Electrochemical Test

Figure 7.3 depicts the SEM micrographs of bainitic and pearlitic steels following a polarization test in NaCl solution. Despite the fact that all the analysed samples have the identical composition, with modest variations in carbon and nickel mass%, they demonstrate varied mechanisms and extent of corrosion damage. This might be ascribed to the variation in microstructure as well as proportions of bainite and RA in bainitic steel. Figure 7.3(a) relates to sample B12VA-1, which demonstrates the existence of cotton ball-type corrosion products; RA exhibits a blocky arrangement with a shallower appearance, and bainite has a somewhat more grooved look. As illustrated in Figure 7.3(b), as Aus. time increases, the volume percentage of RA drops, and a homogenous passive layer with cotton-like corrosion products forms in sample B12VA-2. Figure 7.3(c) illustrates the strong pitting and excessive cracking in the passive layer of the P12VA sample. Figure 7.3(d) depicts SEM micrographs of the polarized sample B14VA-1, which has a greater volume proportion of RA, revealing severe dissolution of blocky RA islands denoted by a yellow circle, cotton-like corrosion products, and fissures in the passive layer. The corrosion morphology of sample B14VA-2 is similar to that of sample B12VA-1, but the dissolution of the bainite matrix increases (Figure 7.3(e)). The morphology of corrosion products of P14VA depicted in Figure 7.3(f), which demonstrates a similar morphology to that of P12VA, but with an increase in intensity of fracture and pits. Figure 7.3(g) depicts the SEM morphology of corrosion products of the sample B15VA-1, which displays a homogenous passive layer, a greater quantity, and a modest dissolution of RA and bainite.

Sample B15VA-2 displays a homogeneous distribution of passive layer throughout the surface of the sample and the corrosion products resembling cotton balls (Figure 7.3(h)). Figure 7.3(i) exhibits the morphology of corrosion product of polarized P15VA samples, which indicates a smaller number of pits than P12VA and P14VA samples, as well as more cotton-ball-like features.

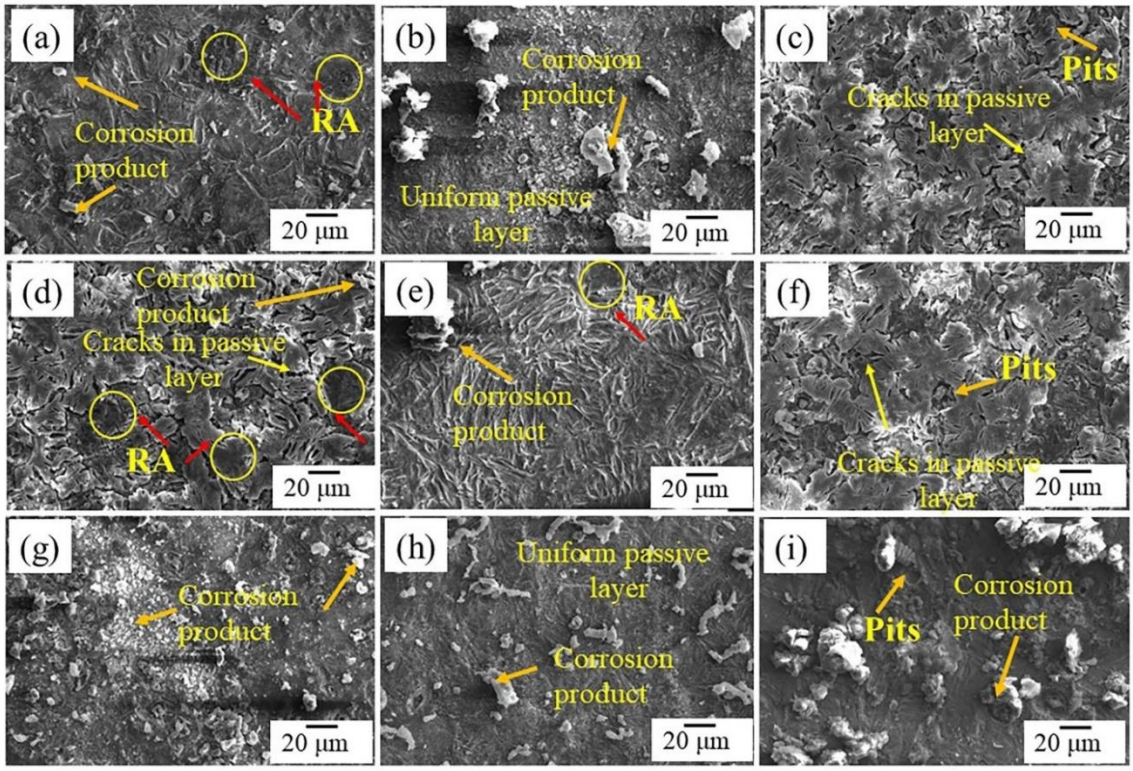


**Figure 7.3** SEM secondary electron images (SEIs) of the corroded surfaces after electrochemical test of the austempered ( at 250°C) bainitic steel (a) B12VA-1, (b) B12VA-2, (d) B14VA-1, (e) B14VA-2, (g) B14VA-1, and (h) B15VA-2 and also, pearlitic steel (at 550°C): (c) P12VA, (f) P14VA, and (i) P15VA.

## 7.2 IMMERSION TEST IN AQUEOUS 3.5% NaCl

### 7.2.1 Weight Loss Measurement

Table 7.3 displays the average value of weight loss (mg/cm$^2$) and corrosion rate (mm/y) of the tested steels after immersion for 30 days in an aqueous 3.5% NaCl solution. For reproducibility, three distinct samples for each condition were tested. The weight loss is used to compute corrosion rate (mm/y) using Equation (2.12). Figure 7.4 depicts the fluctuation in weight loss over the course of 30 days at 7-day intervals.

In the absence of a passive layer, all samples corroded significantly within the first seven days of the immersion test, resulting in considerable weight loss. Corrosion-related weight loss reduces each week and reaches a minimum in the fourth week (Table 7.3). The sample B15VA-2 demonstrates little weight loss over the course of 30 days and enhanced corrosion resistance. Static polarization and impedance spectroscopy reveal the pattern of variation in corrosion rates for the studied steels (Tables 7.1 and Table 7.2), similar to the trend observed during immersion tests (Table 7.3) (Figure 7.5b). The corrosion rate of bainitic steels lowers steadily as the Aus. time rises. Electrochemical test reveals a similar tendency for pearlitic steels.

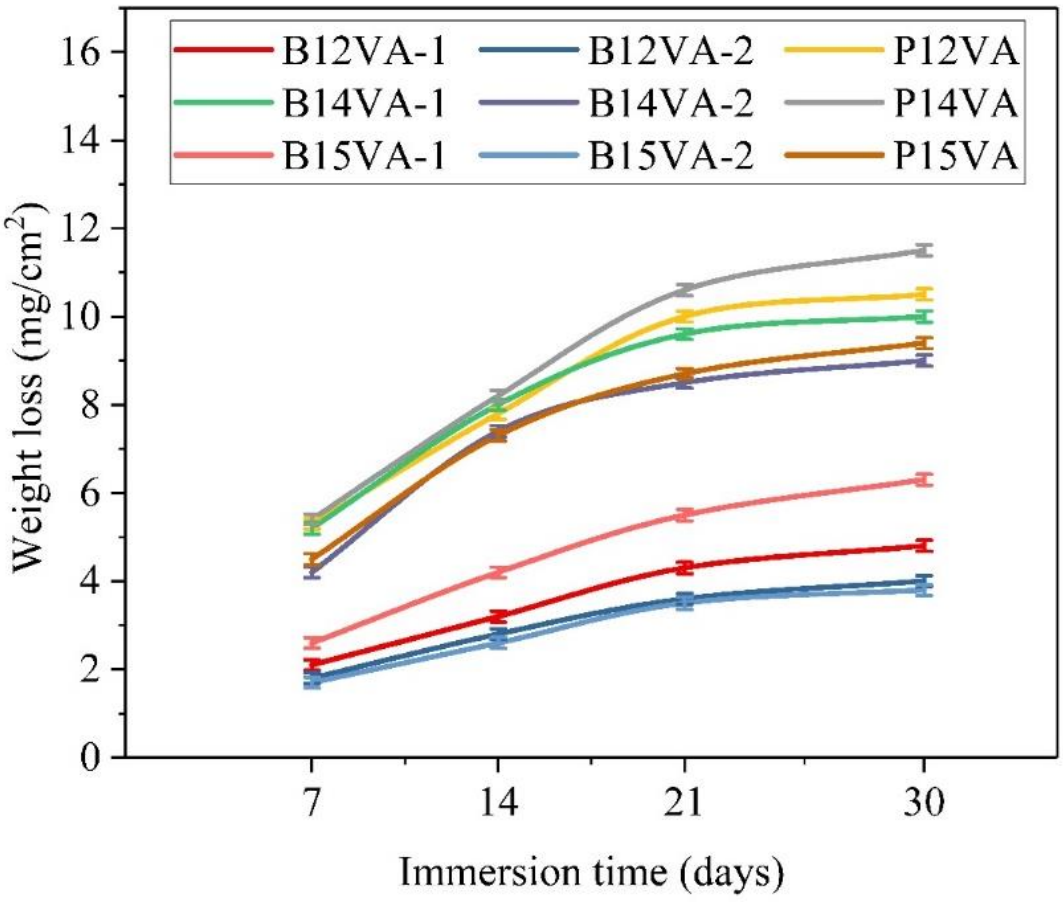


**Figure 7.4** Variation of the weight loss (mg/cm$^2$) of the bainitic and pearlitic steel samples during static immersion test.

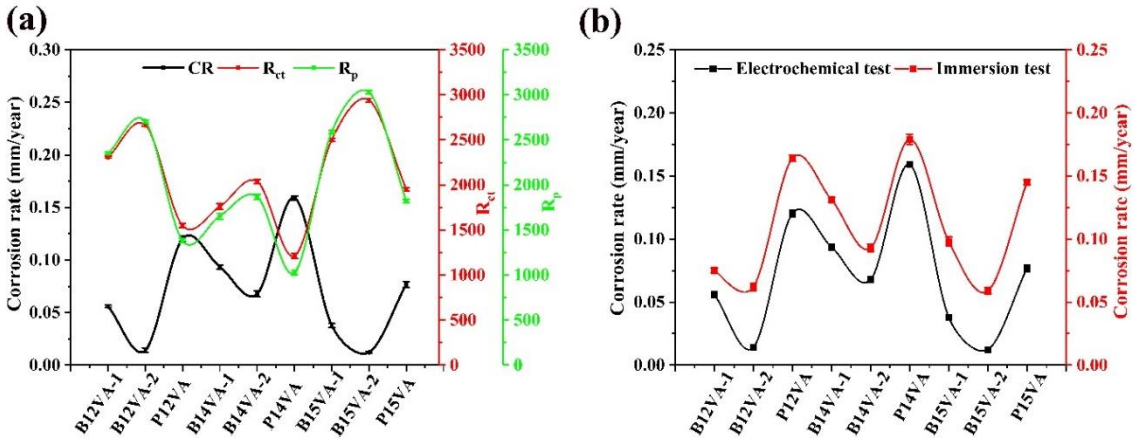


**Figure 7.5** (a) variation of the corrosion rate (CR), charge transfer resistance ($R_{ct}$), and polarization resistance ($R_p$) obtained after the electrochemical test, (b) trends of corrosion rate after electrochemical and immersion test of the austempered bainitic steel and pearlitic steel samples

**Table 7.3** Weight loss measurement during immersion in 3.5% NaCl solution for 30 days and corrosion rate(CR) after 30 days of immersion test of the austempered bainitic and patented pearlitic steels.

| Samples | Wt. loss ($mg/cm^2$) (7 days) | Wt. loss ($mg/cm^2$) (14 days) | Wt. loss ($mg/cm^2$) (21 days) | Wt. loss ($mg/cm^2$) (30 days) | CR (mm/year) |
|---|---|---|---|---|---|
| B12VA-1 | 2.1±0.12 | 3.2±0.13 | 4.3±0.12 | 4.8±0.10 | 0.075±0.001 |
| B12VA-2 | 1.8±0.13 | 2.8±0.12 | 3.6±0.11 | 4.0±0.10 | 0.062±0.002 |
| P12VA | 5.3±0.11 | 7.8±0.13 | 10±0.10 | 10.5±0.12 | 0.164±0.002 |
| B14VA-1 | 5.2±0.14 | 8±0.13 | 9.6±0.14 | 10.0±0.11 | 0.131±0.003 |
| B14VA-2 | 4.2±0.11 | 7.4±0.12 | 8.5±0.12 | 9.0±0.12 | 0.093±0.002 |
| P14VA | 5.4±0.10 | 8.2±0.11 | 10.6±0.13 | 11.5±0.14 | 0.179±0.002 |
| B15VA-1 | 2.6±0.13 | 4.2±0.13 | 5.5±0.14 | 6.3±0.15 | 0.098±0.003 |
| B15VA-2 | 1.7±0.10 | 2.6±0.10 | 3.5±0.12 | 3.8±0.11 | 0.059±0.001 |
| P15VA | 4.5±0.12 | 7.3±0.12 | 8.7±0.11 | 9.4±0.13 | 0.1447±0.002 |

### 7.2.2 Morphology of Products of Corrosion After Immersion Test

SEM analysis of 30 days immersion tested samples reveal several forms of rust morphologies (Figure 7.6). The corrosion products developed on the samples are fairly uniform, and the outer corroded surface seems to be fractured (passive layer crack) and

linked across the corroded surface. Figure 7.6a displays the rust morphology of sample B12VA-1, which consists of a compact passive layer with a few fractures and corrosion products resembling cotton balls. Similarly, the B12VA-2 sample exhibits a homogeneous passive layer with extremely small fractures and corrosion products (Figure 7.6b). Figure 7.6c depicts the rust morphology of the P12VA sample, which exhibits the existence of widespread corrosion products and large-scale fractures on the corrosion layer. Figure 7.6d depicts the corrosion surface of the B14VA-1 sample, which reveals large-sized fractures across the corrosion layer as well as cotton ball like corrosion products. The B14VA-2 sample displays a lesser number of large-sized cracks in the corrosion layer (Figure 7.6e), as well as corrosion products with a comparable shape. Figure 7.6f depicts the rust morphology of a P14VA sample, which demonstrates a morphology comparable to that of P12VA but with an increase in corrosion products. As illustrated in Figure 7.6g, sample B15VA-1 has a homogenous, compact passive layer with extremely thin fractures and a limited amount of corrosion products resembling cotton balls. The compact rust morphology of sample B15VA-2, seen in Figure 7.6h, indicates a homogenous, compact passive layer comprised of very fine cotton ball-like corrosion products. Figure 7.6i depicts the corrosion rust morphology of the P15VA sample, which demonstrates a modest number of large-sized fractures in addition to widespread corrosion products.

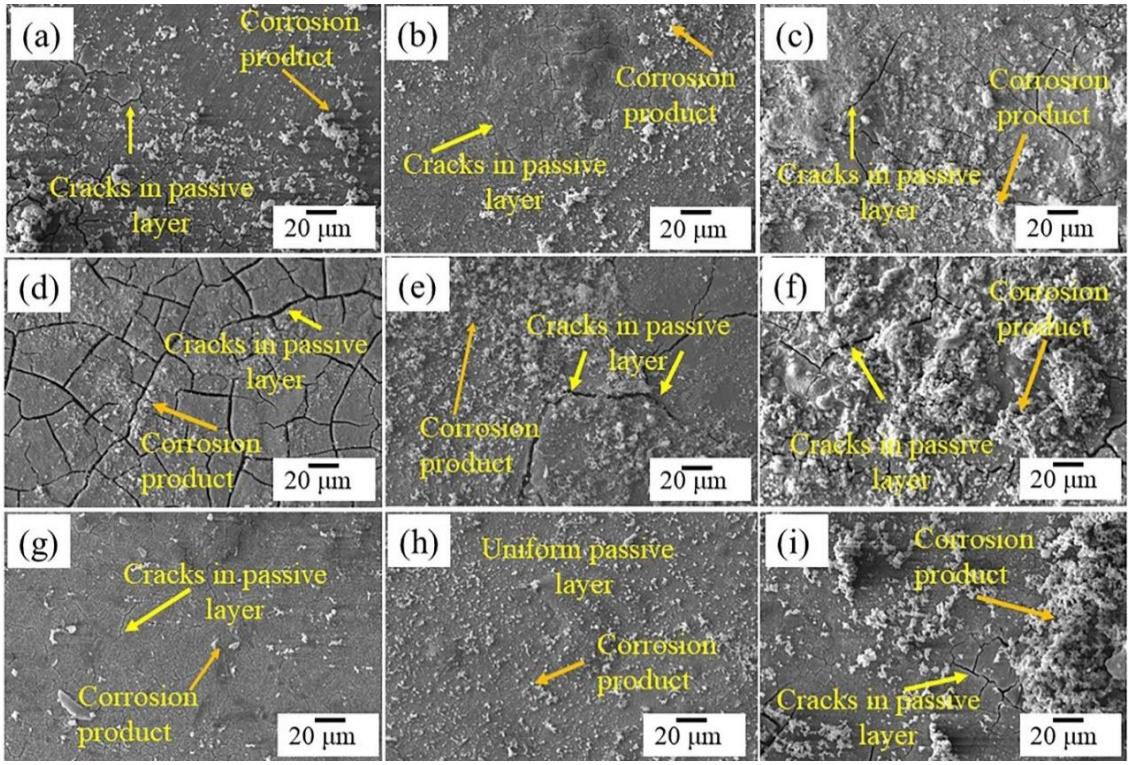


**Figure 7.6** SEM secondary electron images (SEIs) of the corroded surfaces after 30 days of immersion test of the austempered ( at 250°C) bainitic steel (a) B12VA-1, (b) B12VA-2, (d) B14VA-1, (e) B14VA-2, (g) B14VA-1, and (h) B15VA-2 and also, pearlitic steel (at 550°C): (c) P12VA, (f) P14VA, and (i) P15VA.

Figures 7.7a-i reveal the area scan EDS analysis of the corrosion passive layer (of Figure 7.6a-i) of the samples immersed in 3.5% NaCl solution for 30 days. EDS plots show the peaks of constituent elements responsible for the formation of corrosion products, namely Fe, Cr, Mo, Co, Ni, C, Si, Mn, Al, Na, and Cl. The area scan EDS analysis of the 30 days immersed samples reveal that the increase in peak intensity of oxide with the Aus. time and reduced peak intensity is observed in pearlitic samples. The peak intensity of Cr, Co, Si, Mn, Mo, Al and Fe follows the same trend as oxide peaks in all the samples, but the reduced peak intensity of Cr is observed in the samples B14VA-1, B14VA-2, P14VA and P15VA. As Ni is present in very fewer amounts (~ 0.05 mass%) in B12VA and B14VA, reduced peak intensity of Ni is observed in the samples B12VA-

1, B12VA-2, P12VA, B14VA-1, B14VA-2 and P14VA. Sample B15VA-2 shows higher peak intensity of Ni than B15VA-1 and P15VA samples.

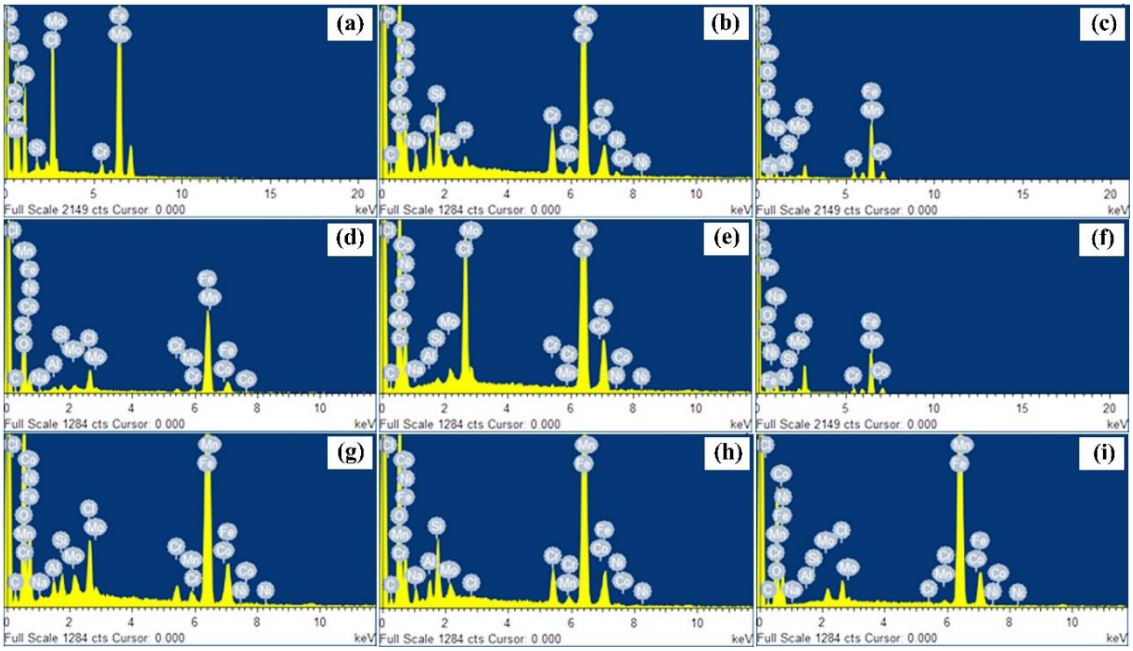


**Figure 7.7** Energy dispersive spectroscopy (EDS) of the corroded surfaces after 30 days immersion test of the austempered ( at 250$^{o}$C) bainitic steel (a) B12VA-1, (b) B12VA-2, (d) B14VA-1, (e) B14VA-2, (g) B14VA-1, and (h) B15VA-2 and also, pearlitic steel (at 550$^{o}$C): (c) P12VA, (f) P14VA, and (i) P15VA in aqueous 3.5% NaCl solution.

Immersion of B15VA-2 in aqueous 3.5% NaCl solution for 30 days produces compact passive layer. The analysis of EDS spectrum (Figure 7.8c) confirms the passive layer to be $Fe_3O_4$ (indicated in Figure 7.8a). Some cotton ball like corrosion products also appeared on the surface of the corroded sample, as is clearly seen in magnified SE image (Figure 7.8b). The EDS analysis (Figure 7.8b') of it confirmed the formation of $Fe_2O_3$ on the surface of the corroded sample. There are also small amount of FeOOH present in the corroded surface which is confirmed from the EDS analysis (Figure 7.8d).

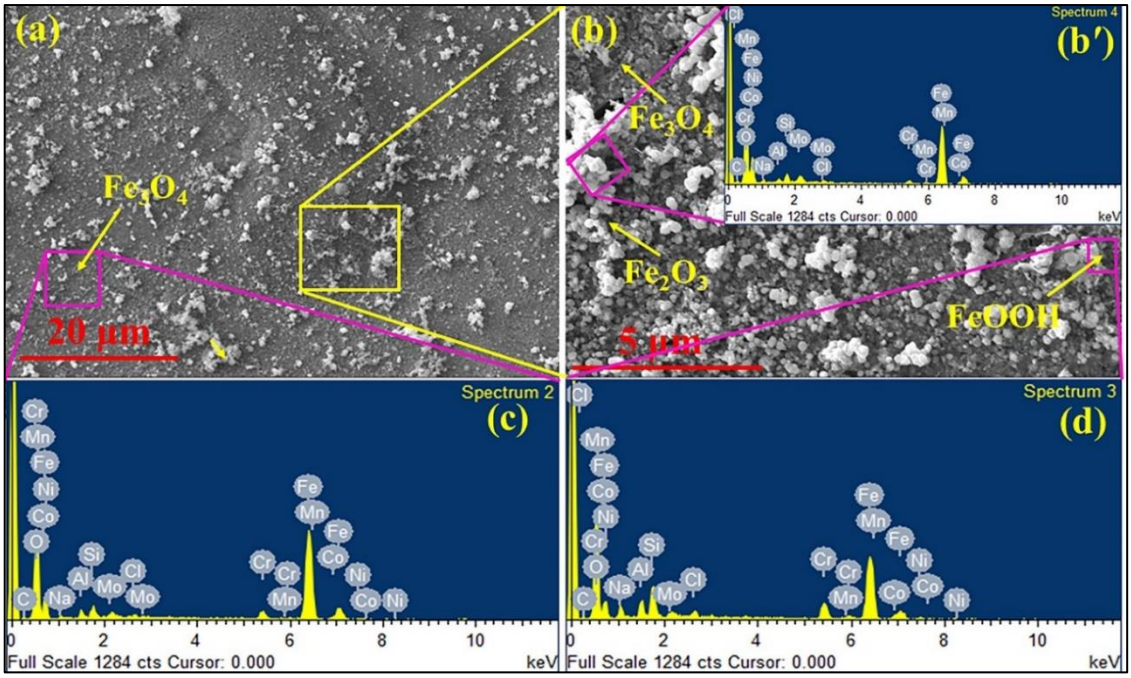


**Figure 7.8** SEM secondary electron images (SEIs) of the corroded surfaces after 30 days of immersion test of the Bainitic steel: (a) B15VA-2, (b) Magnified SEI of selected area of Figure 7.8(a) indicated by yellow rectangle, (c) EDS spectra of pink colour marked area, and (d) EDS spectra of pink colour marked area. Inset in Figure 7.8(b).

Detailed analysis of corrosion product in SEM equipped with EDS of the sample P15VA is also performed. Figure 7.9a depicts the SEIs of corroded surface of P15VA sample and it reveals similar features of corrosion products $Fe_3O_4$, with higher amount of FeOOH and $Fe_2O_3$. Figure 7.9b corresponds to the magnified view of Figure 7.9a in which all the above corrosion products are indicated which are confirmed by the EDS analysis of selected area (Figure 7.9b′ in inset) for FeOOH. Analysis of EDS spectras of pink colour rectangle areas (Figures 7.9c & d) confirm the formation of Fe-based oxides mainly FeOOH, $Fe_3O_4$ and $Fe_2O_3$ as shown in Figure 7.9b for P15VA.

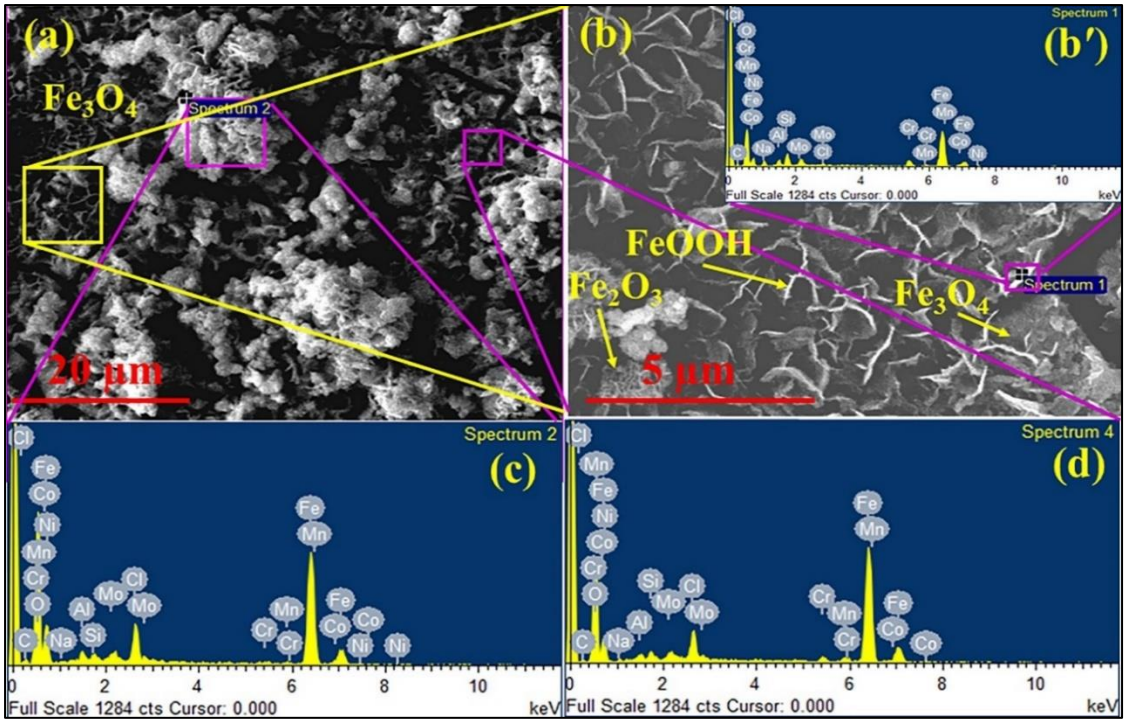


**Figure 7.9** SEM secondary electron images (SEIs) of the corroded surfaces after 30 days of immersion test of the pearlitic steel (at 550°C): (a) P15VA, (b) Magnified SEI of yellow colour rectangle area of Figure 7.9(a), (c) EDS spectra of pink colour marked area, and (d) EDS spectra of pink colour marked area. Inset Figure 7.9(b).

## 7.3 DISCUSSION

### 7.3.1 EIS and Potentiodynamic Polarization

Each Nyquist figure incorporates both inductive and capacitive loops. A double electrical layer is often described as a capacitance component, but when the dispersion effect is included, a constant phase angle element CPE is substituted for the capacitance. The following formula Equation (7.1) describes the impedance of CPE [201].

$$Z = \frac{1}{\gamma'(jw)^n} \tag{7.1}$$

Where γ' is a constant with the unit $\Omega^{-1}.cm^{-2}$, slope of Bode plot is represented by n with values between 0 and 1, and *w* is the angular frequency. If n=0, the component operates as a pure resistor; if n=1, it as a pure capacitor; and if n= -1 as a pure inductor.

Consequently, the model's complete impedance may be described as follows by Equation (7.2).

$$Z = R_S + \frac{1}{\gamma'(\mathrm{jw})^{\,n} + \frac{1}{R_{ct}}} \tag{7.2}$$

Where $R_s$ and $R_{ct}$ are the solution resistance and charge transfer resistance, respectively, and the parameters of the fitted impedance data of bainitic and pearlitic steels are presented in Table 7.2.

The $R_s$ values of NaCl solution are similar for all the electrochemical tests excluding a few pearlitic steel samples, whose $R_s$ values deviate from other samples in a range of ±4 Ω/cm$^2$. The fluctuation of the $R_s$ value in aqueous NaCl solution is in line with the literature [114, 124, 202]. The association between the dissolution behaviour of the studied steels and the $R_{ct}$ values is noteworthy. Consequently, greater $R_{ct}$ values imply superior corrosion resistance. The general pattern found in the fluctuation of $R_{ct}$ (Table 7.2) is exactly the reverse of the trend reported in the corrosion rate (Table 7.1) for steels (Figure 7.5(a)). As the $R_{ct}$ increases, the corrosion rate decreases, and vice versa.

The Bode phase graphs (Figure 7.2(c)) reveal that at extremely high frequencies, the phase angle reduces to 0 degrees for the studied steels, suggesting that the $R_s$ dominates the impedance in this frequency range. In addition, the phase angle is observed to decrease in the low-frequency zone, which might be ascribed to the $R_P$. Bode phase plot maxima ranges from 62 to 74° for all bainitic steels, although the pearlitic steel inflection point is in the range of 61 to 71°. The phase angle associated with the inflection point is wider in the range of 61-74° throughout a narrow frequency zone. It implies that all bainitic and pearlitic rail steels strive for a capacitive response. Consequently, this may be an indicator of the development of a thin passive film on the studied steels, which

is predicted to provide superior resistance to corrosion [121]. The frequency-independent horizontal parts of the Bode magnitude plots are suggesting a response of pure resistance, as represented in Figure 7.2(b). The middle region of bainitic steels is wider than that of pearlitic steels. According to this finding, the impedance of the bainitic samples has improved, which suggests that bainitic steels have a more stable passive film than pearlitic steels.

All the bainitic steel samples reveal a decrease in corrosion rate with an increase in Austempering time. This is due to the fact that there is a steady change in the galvanic effect. In bainitic steel samples, retained austenite and bainite act as a galvanic couple and lead to galvanic cell corrosion and ferrite and cementite act as a galvanic couple in pearlitic steel samples. Table 3.1 demonstrates clearly that the volume percentages of retained austenite decrease with Austempering time. Sample B14VA-1 has a higher volume fraction of retained austenite, has undergone more galvanic effect and shows a higher corrosion rate. When the rate of corrosion in steels increases, the influence of galvanic cell corrosion becomes more apparent than it ever has before. Previous research has shown that the C content of the retained austenite is higher than that of the bainite phase [124] and that the marginal selective dissolution in the retained austenite is the result of galvanic cell corrosion [124, 203, 204]. With an increase in Austempering time, the volume fraction of retained austenite and size of blocky austenite decrease causing a reduction in galvanic couple and, therefore, the corrosion resistance of the bainitic steel enhanced with increasing Austempering time. In pearlitic steel samples, lamellar colonies of cementite and ferrite are present. There is a huge effect of the galvanic pair among cementite and ferrite which therefore leads to an increase in galvanic corrosion in pearlitic steel samples. The galvanic corrosion led to selective dissolution in cementite

in pearlitic steel samples [121]. Therefore, bainitic steel is more resistant to corrosion than pearlitic steel.

### 7.3.2 XPS Analysis

When it concerns to the corrosion performance, the chemistry of the surface layers is of significant interest. Consequently, XPS was utilized in order to analyze the chemical composition of the surface. The XPS survey spectrum of the surfaces can be seen in Figure 7.10, which is a reflection of the nominal composition of the corrosion products.

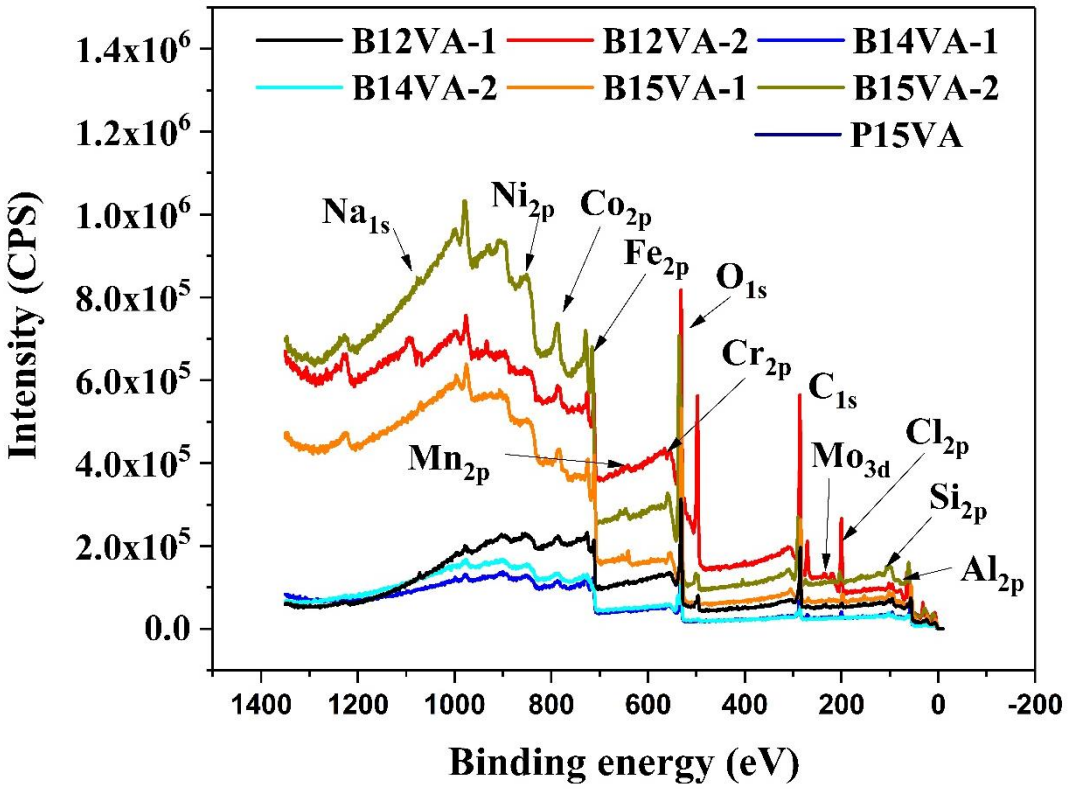


**Figure 7.10** XPS survey spectrum of the corroded surfaces after 30 days immersion test of the austempered ( at 250°C) bainitic steels: B12VA-1, B12VA-2, B14VA-1, B14VA-2, B14VA-1, and B15VA-2 and also, pearlitic steel (at 550°C): P15VA.

The concentration of elements derived from these spectra suggests the development of Fe, C, Si, Al, Ni, Mn, Co, Cr, and Mo oxides and their hydroxides in the passive layer of the corroded sample. It is evident from the survey spectrum that an

increase in Aus. time results in an enhanced passive layer by sufficient oxide formation due to corrosion displaying higher intensity counts in the spectra. The XPS spectrum of Fe 2p , and O 1s are revealed in Figure 7.11 to Figure 7.19.

The XPS spectrograph's peak-fitting results of Fe $2p_{3/2}$ of the samples B12VA-1, B12VA-2, B14VA-1, B14VA-2, B15VA-1, B15VA-1 and P15VA are shown in Figure 7.11(a-g) respectively. The spectrum of $Fe2p_{3/2}$ deconvoluted into the numerous constituent peaks depicting the bivalent ($Fe^{2+}$) species and trivalent ($Fe^{3+}$) species hydroxyl ($OH^-$). Mainly, the corrosion products consisted of FeO (708.1 ± 0.2 eV), $Fe_2O_3$ (709.3 ± 0.3 eV), FeOOH (711.8 ± 0.2 eV) and $Fe_3O_4$ ($Fe^{2+}$ at 710.9±0.3 eV and $Fe^{3+}$ at 712.4±0.4 eV). The presence of FeO is seen only in B14VA-1, B15VA-1and B15VA-2 samples. $Fe_2O_3$ peak is present only in B15VA-1 sample. The BE corresponding to 712.80±0.3 and 714.40±0.2 eV ascribed to the shake-up satellite peaks. The peak intensity of oxides and hydroxides of Fe is higher for B15VA-2 samples. The XPS spectrograph of O1s is shown in Figure 7.12(a-g). The presence of oxygen in the forms of $O^{2-}$ (530.2 ± 0.2 eV), $OH^-$ (531.0 ± 0.2 eV), and $H_2O$ (533.3±0.2 eV) suggested that the passive film was mostly made up of metal oxide and hydroxide. B15VA-2 shows higher peak intensities of oxide and hydroxide.

The XPS spectrograph of Cr 2p3/2 is demonstrated in Figure 7.13(a-g). Cr (metal) (574.1 ± 0.2 eV), $Cr_2O_3$ (576.3 ± 0.3 eV), CrOOH (577.0 ± 0.3 eV), and $CrO_3$ (578.1 ± 0.2 eV) and $CrO_4^{2-}$ (579.3±0.2) were the primary constituents of Cr in the passive films formed in the samples B12VA-1, B12VA-2, B15VA-1 and B15VA-2 immersed in the NaCl solution for 30 days. No XPS peaks of Cr were observed in the passive layer of the samples B14VA-1, B14VA-2 and P15VA. The intensity of oxides and hydroxides of Cr is higher for the sample B15VA-2.

Figure 7.14(a-g) displays peak fitting of $Co_{2p}$. In $Co_{2p}$ spectra, the peaks at 782.3±0.2 eV ascribed to the binding energies of $Co^{2+}$ producing CoO and BE 786.0±0.3 eV ascribed to the shake-up satellite peaks. The sample B15VA-2 depicts higher peak intensity of the oxides of Co.

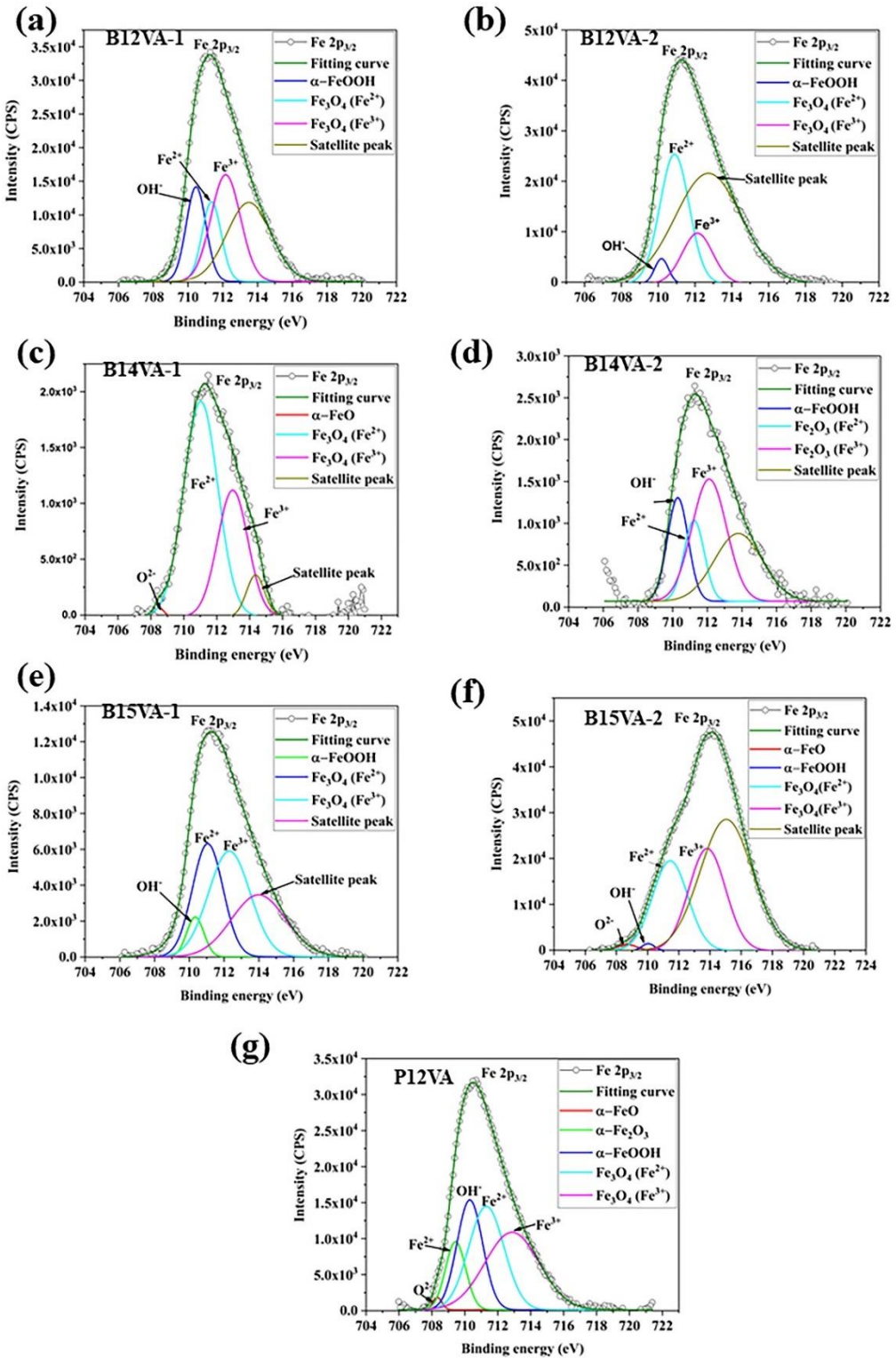


**Figure 7.11** The XPS spectrograph's peak-fitting results of Fe $2p_{3/2}$ after 30 days immersion test of the austempered ( at 250°C) bainitic steels samples: (a) B12VA-1, (b) B12VA-2, (c) B14VA-1, (d) B14VA-2, (e) B14VA-1, and (f) B15VA-2 and also, pearlitic steel (at 550°C): (g) P15VA.

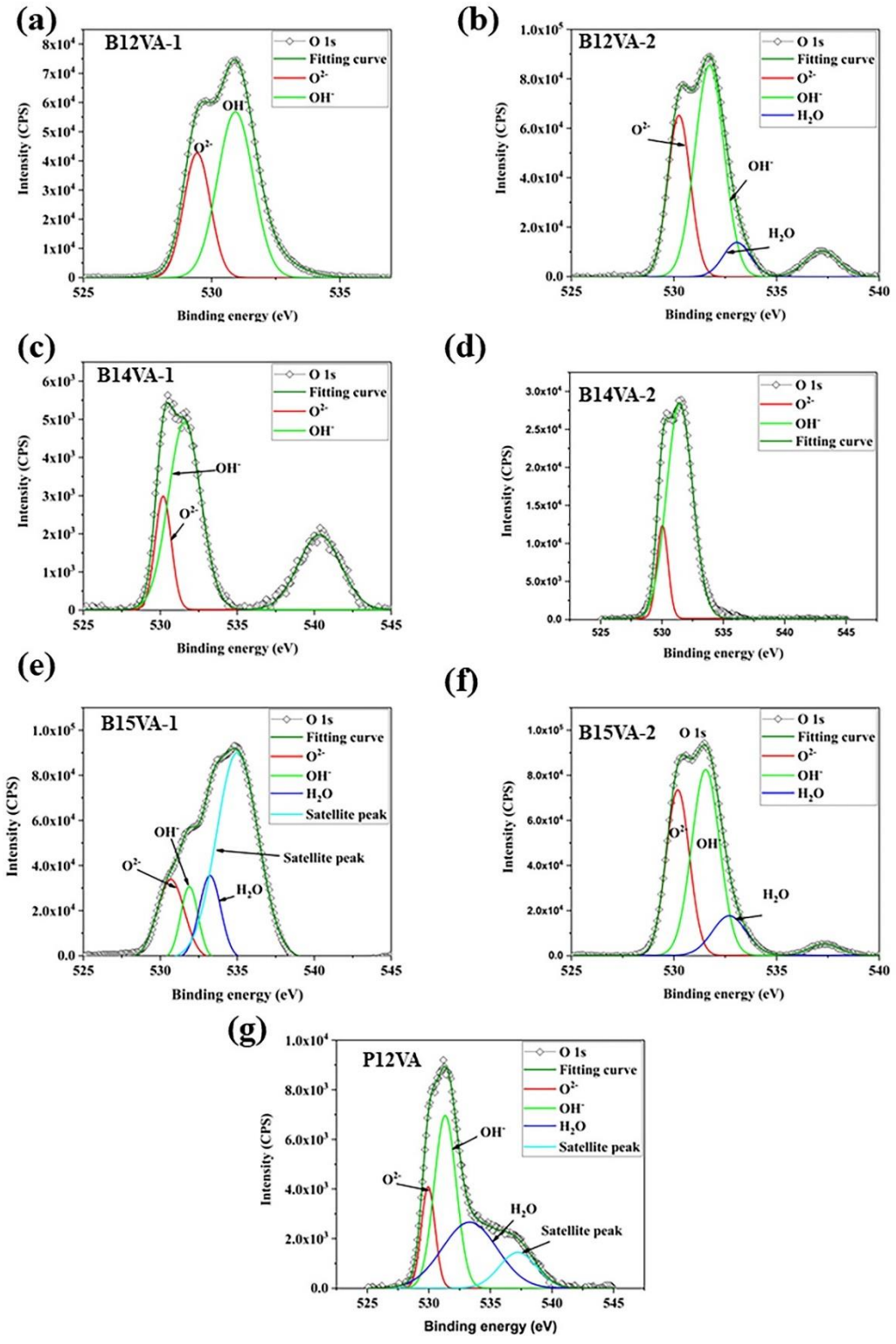


**Figure 7.12** The XPS spectrograph's peak-fitting results of O 1s after 30 days immersion test of the austempered ( at 250°C) bainitic steels samples: (a) B12VA-1, (b) B12VA-2, (c) B14VA-1, (d) B14VA-2, (e) B14VA-1, and (f) B15VA-2 and also, pearlitic steel (at 550°C) of (g) P15VA.

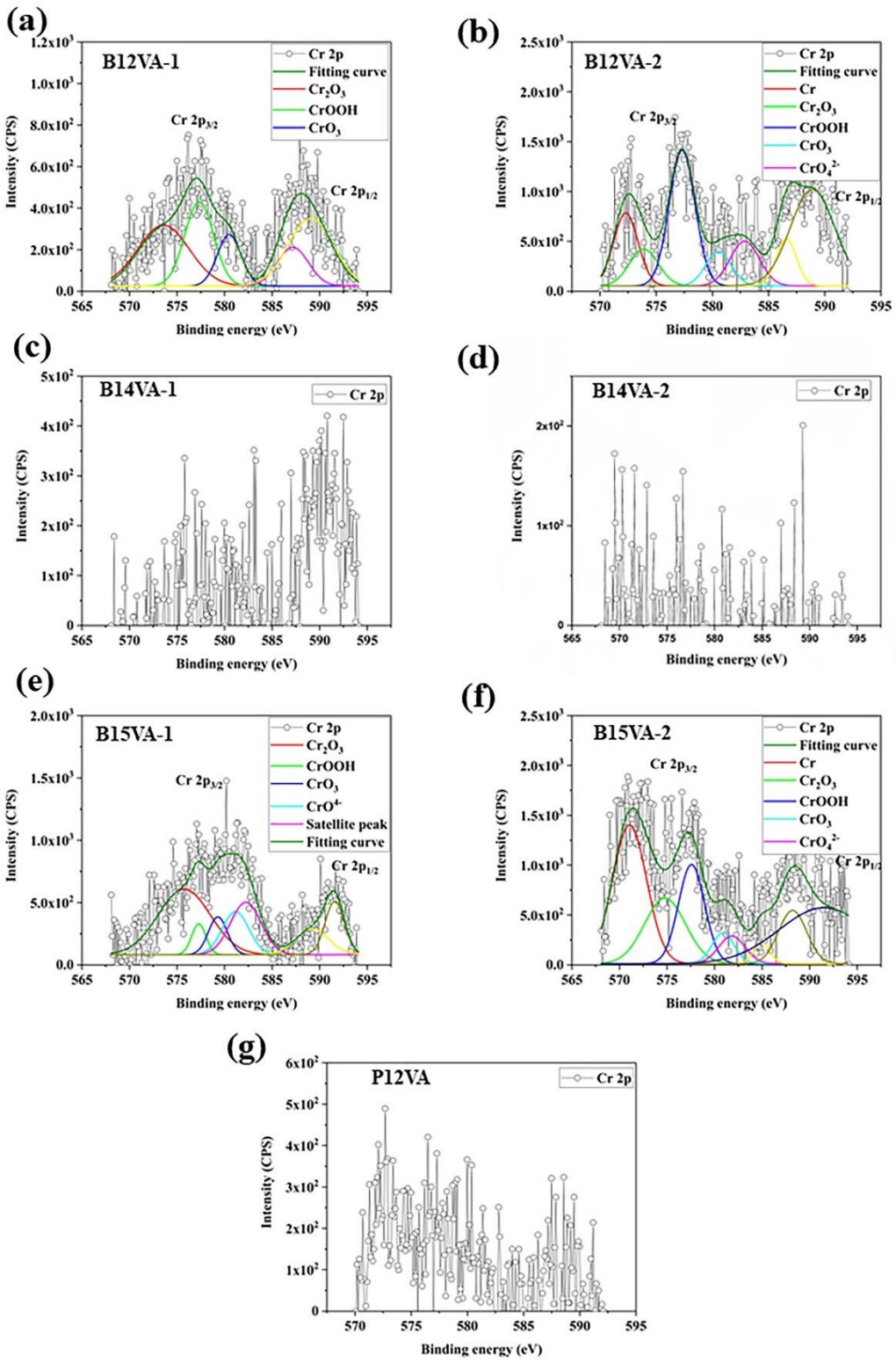


**Figure 7.13** The XPS spectrograph's peak-fitting results of Cr 2p after 30 days immersion test of the austempered (at 250°C) bainitic steels samples: (a) B12VA-1, (b) B12VA-2, (c) B14VA-1, (d) B14VA-2, (e) B14VA-1, and (f) B15VA-2 and also, pearlitic steel sample (at 550°C): (g) P15VA in an aqueous 3.5% NaCl solution.

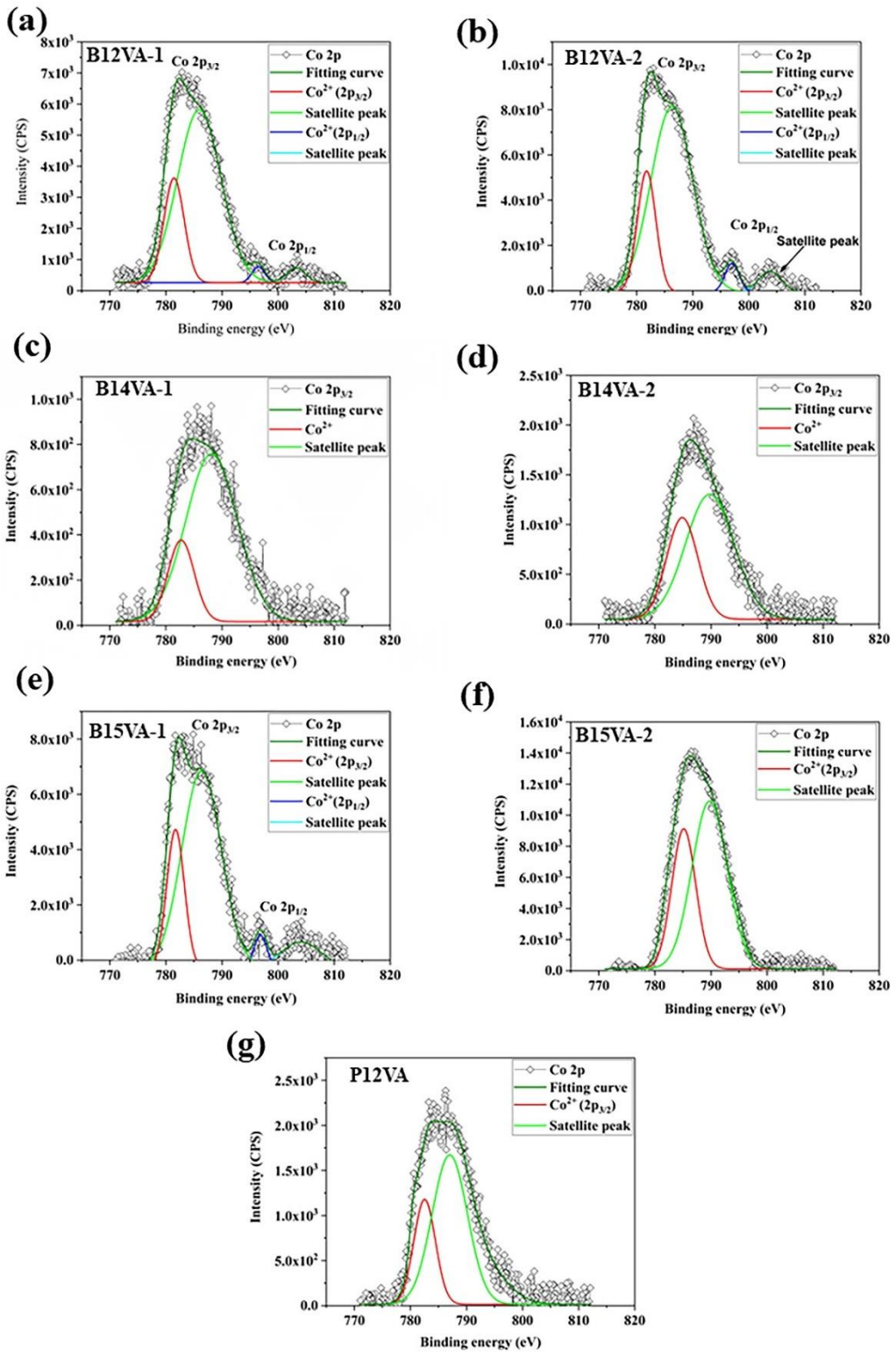


**Figure 7.14** The XPS spectrograph's peak-fitting results of Co 2p after 30 days immersion test of the austempered ( at 250$^{o}$C) bainitic steels samples: (a) B12VA-1, (b) B12VA-2, (c) B14VA-1, (d) B14VA-2, (e) B14VA-1, and (f) B15VA-2 and also, pearlitic steel (at 550$^{o}$C): (g) P15VA in an aqueous 3.5% NaCl solution.

Figure 7.15(a-c) displays the results of peak fitting of the XPS spectrograph of Ni 2p3/2 in the samples B15VA-1, B15VA-2 and P15VA respectively. It mainly consists of oxides and hydroxides of Ni in the samples B15VA-1, B15VA-2 and P15VA, respectively. The peak corresponds to 855.7±0.3 eV BE ascribed to $Ni(OH)_2$ in B15VA-1, B15VA-2 and P15VA. The peak at 853.7±0.1 corresponds to NiO in B15VA-2 only and no XPS peaks of oxides and hydroxides of Ni were present in the samples B12VA-1, B12VA-2, B14VA-1 and B14VA-2. Figure 7.16(a-g) depicts the peak fitting of XPS spectrograph of Mo3d. The peaks corresponding to 232.20±0.2 eV BE ascribed to $Mo^{4+}$ (Oxide) and the BE 235.20±0.2 eV is ascribed to $Mo^{6+}$ (Oxide) in the samples B12VA-2, B15VA-1 and B15VA-2 but no XPS peaks of oxides and hydroxides of Mo were seen in the samples B12VA-1, B14VA-1, B14VA-2 and P15VA.

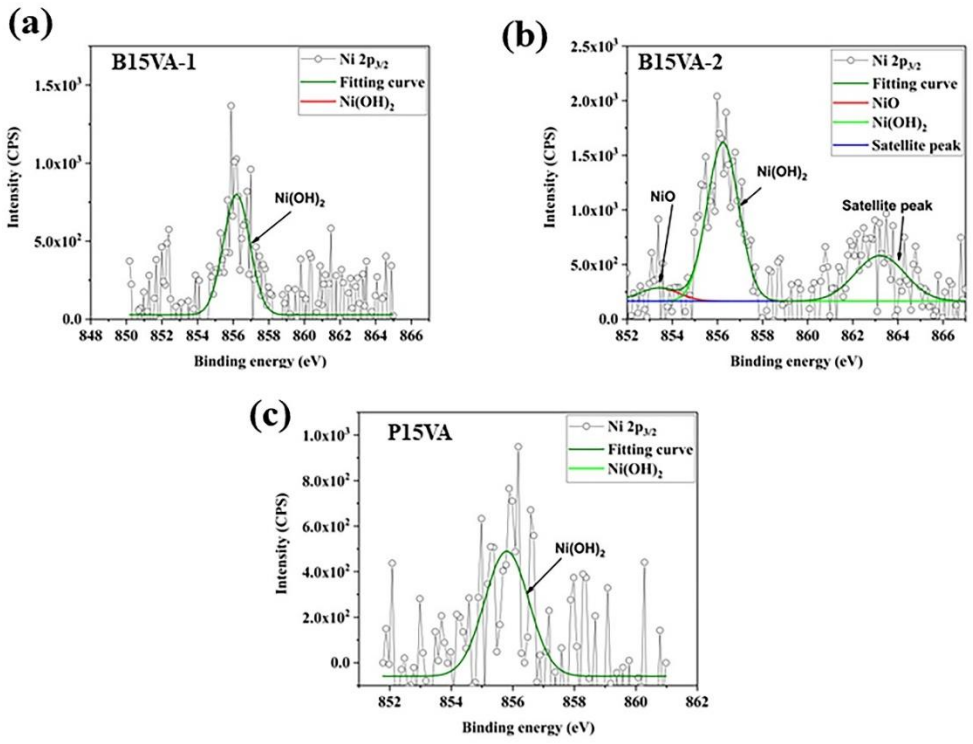


**Figure 7.15** The XPS spectrograph's peak-fitting results of Ni $3p_{3/2}$ after 30 days immersion test of the austempered ( at 250°C) bainitic steels: (a) B15VA-1, (b) B15VA-2 and , pearlitic steel (at 550°C): (c) P15VA in an aqueous 3.5% NaCl solution.

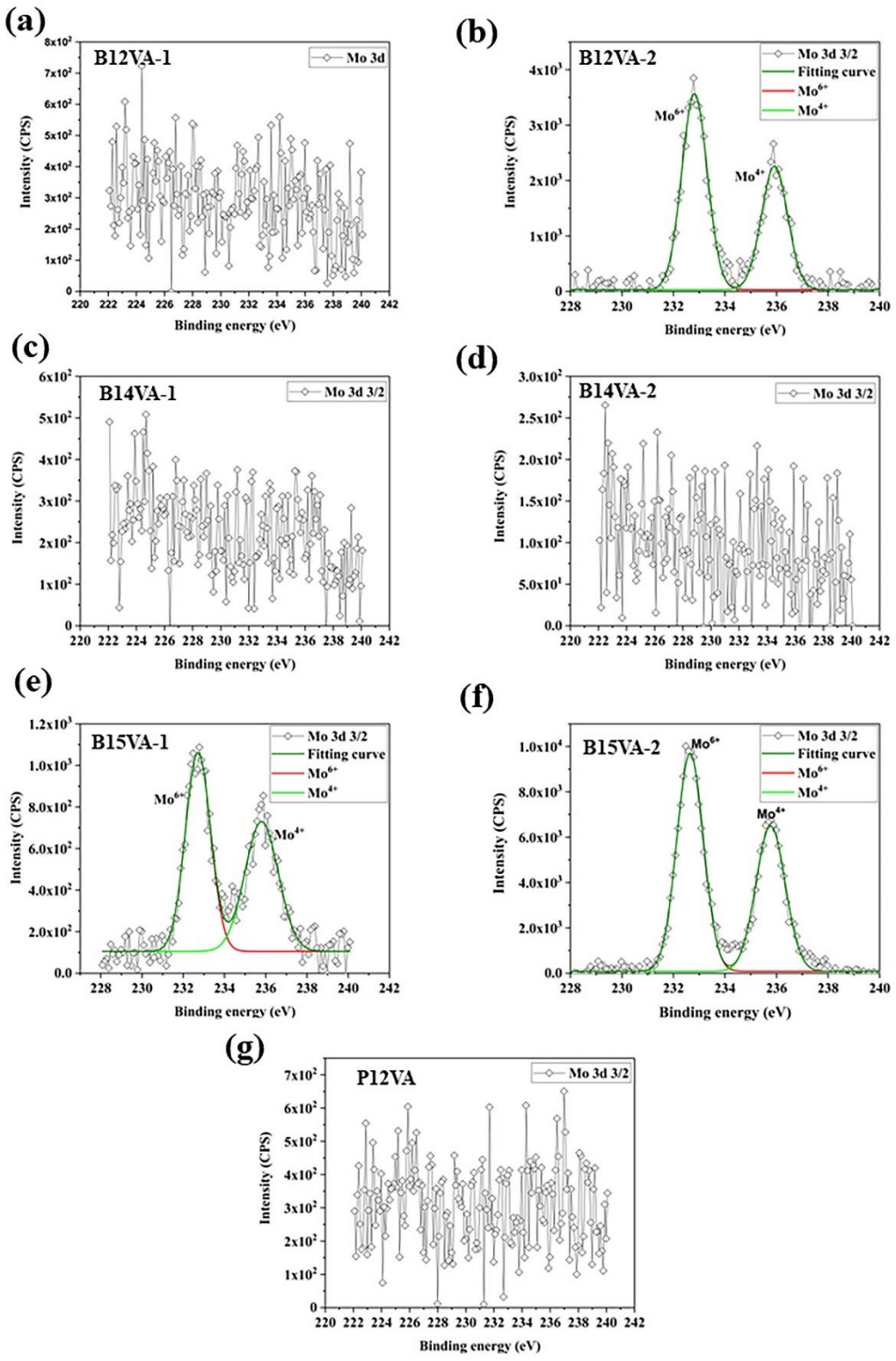


**Figure 7.16** The XPS spectrograph's peak-fitting results of Mo $3d_{3/2}$ after 30 days immersion test of the austempered ( at 250°C) bainitic steels: (a) B12VA-1, (b) B12VA-2, (c) B14VA-1, (d) B14VA-2, (e) B14VA-1, and (f) B15VA-2 and also, pearlitic steel (at 550°C): (g) P15VA in an aqueous 3.5% NaCl solution.

The results of peak fitting of the XPS spectrograph of Al $2p_{3/2}$ are shown in the Figure 7.17(a-g). It mainly consists of $Al_2O_3$ in the passive layer of the samples B12VA-1, B12VA-2, B15VA-1, B15VA-2 and P15VA, corresponding to the BE of 74.6±0.1 eV. Some precipitates of Al were seen in the XPS result of sample P15VA, corresponding to the BE of 72.8±0.1 eV. No XPS peaks of oxides and hydroxides of Al were seen in the samples B14VA-1 and B14VA-2.

Figure 7.18(a-g) depicts peak fitting of the XPS spectrograph of the Mn 2p. It consists of Mn $2p_{1/2}$ and Mn $2p_{3/2}$ peaks but only Mn $2p_{3/2}$ peaks were deconvoluted and indexed. Mn $2p_{3/2}$ mainly consists of oxides (MnO at a BE of 640.3± 0.2 eV) and hydroxides ($Mn(OH)_2$) at a BE of 641.9± 0.3 eV) and BE of 644.3±0.2 eV ascribed to shake-up satellite peaks. There is no XPS peaks of oxides and hydroxides of Mn in the passive layer of the sample B14VA-1.

The XPS peak of Si $2p_{3/2}$ are displayed in Figure 7.19(a-g), which mainly consists of metal Si at a BE of 99.2±0.2 eV and $SiO_2$ (oxides) at a BE of 103.1±0.3 eV in the passive layer of corrosion product of all the samples. The BE 104.9±0.1 eV is ascribed to the shake-up satellite peak in B12VA-1.

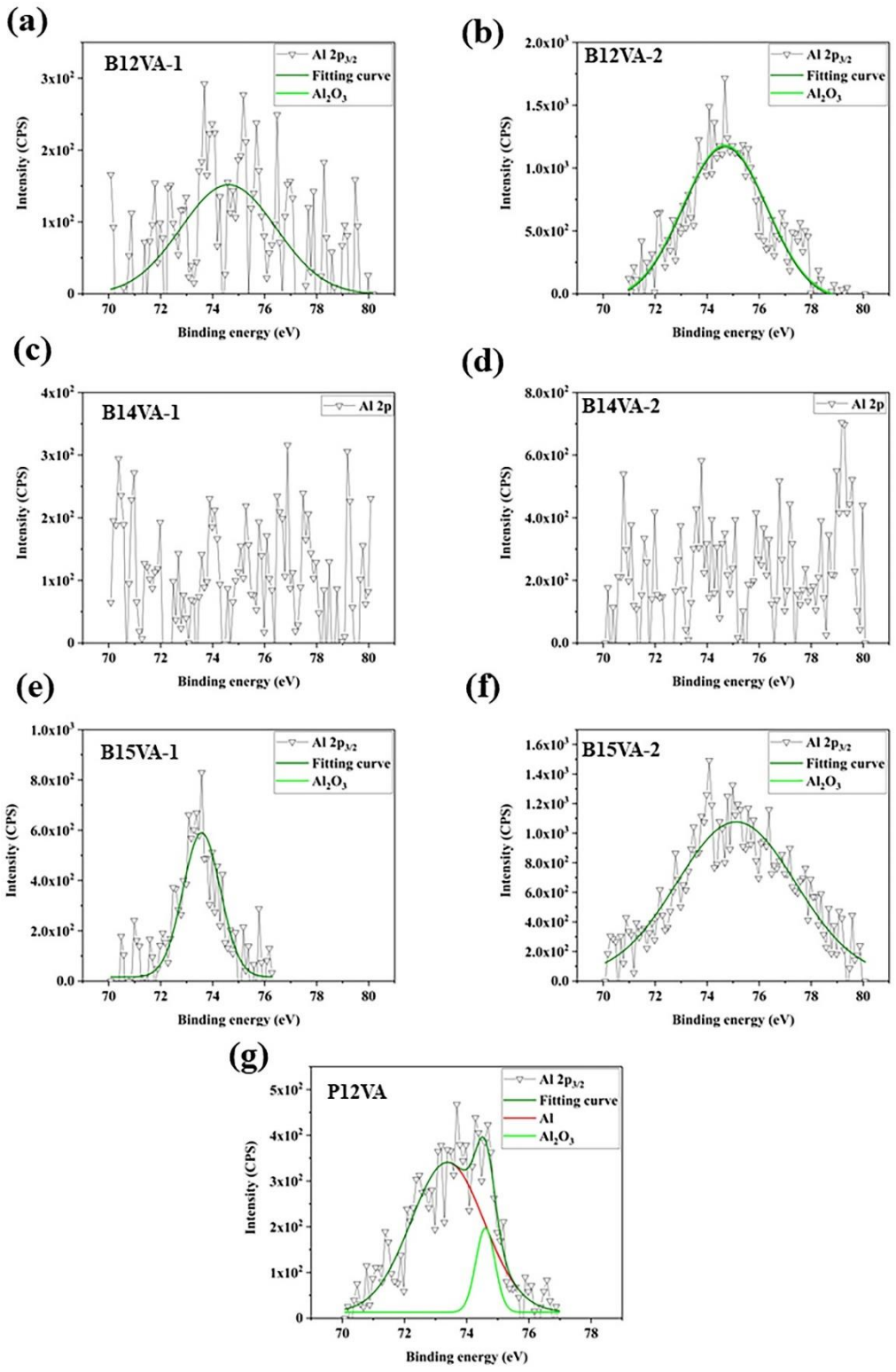


**Figure 7.17** The XPS spectrograph's peak-fitting results of Al $2p_{3/2}$ after 30 days immersion test of the austempered ( at 250°C) bainitic steels samples: (a) B12VA-1, (b) B12VA-2, (c) B14VA-1, (d) B14VA-2, (e) B14VA-1, and (f) B15VA-2 and also, pearlitic steel (at 550°C): (g) P15VA in an aqueous 3.5% NaCl solution.

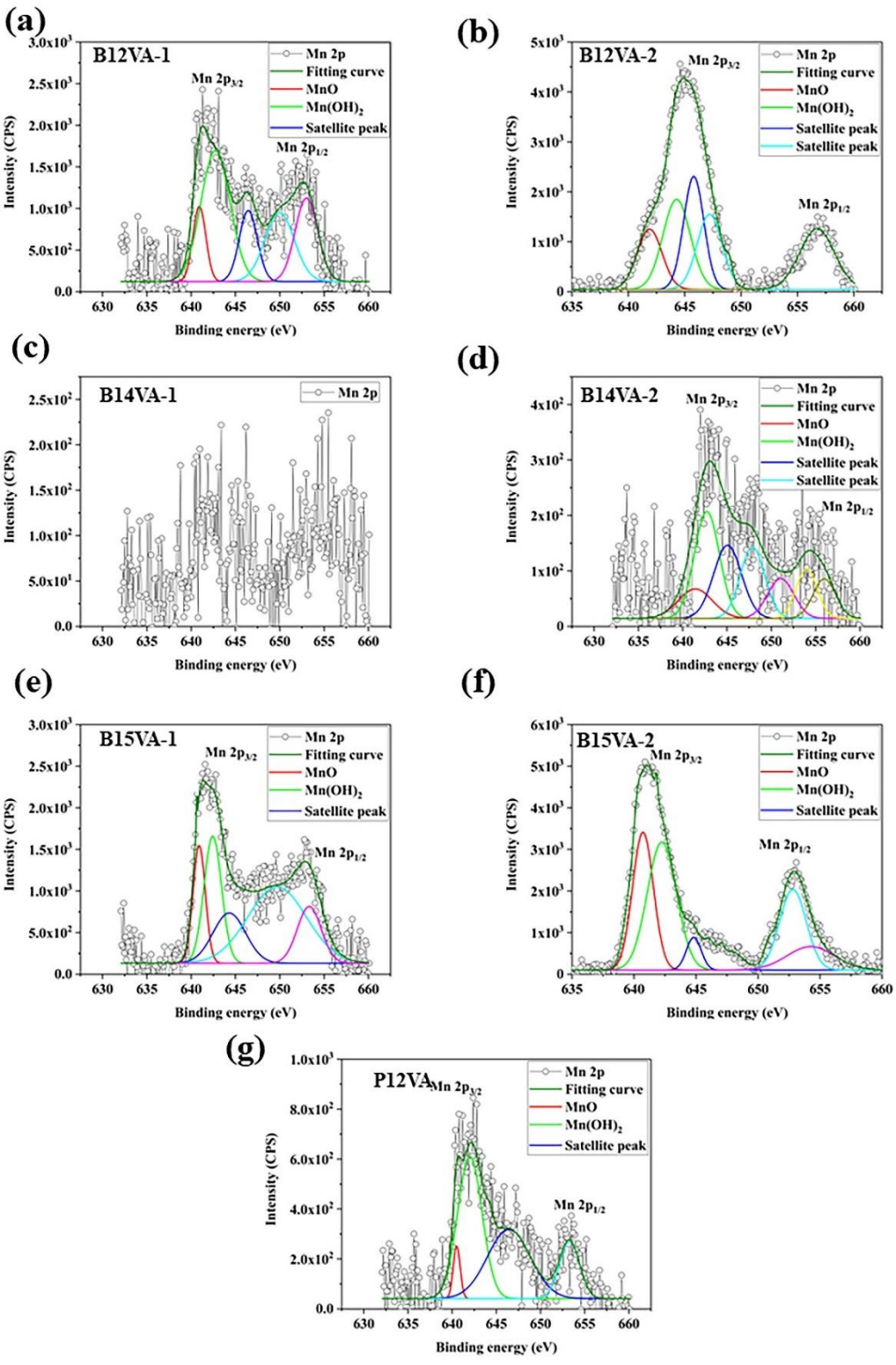


**Figure 7.18** The XPS spectrograph's peak-fitting results of Mn $2p_{3/2}$ after 30 days immersion test of the austempered ( at 250°C) bainitic steels samples: (a) B12VA-1, (b) B12VA-2, (c) B14VA-1, (d) B14VA-2, (e) B14VA-1, and (f) B15VA-2 and also, pearlitic steel (at 550°C): (g) P15VA in aqueous 3.5% NaCl solution.

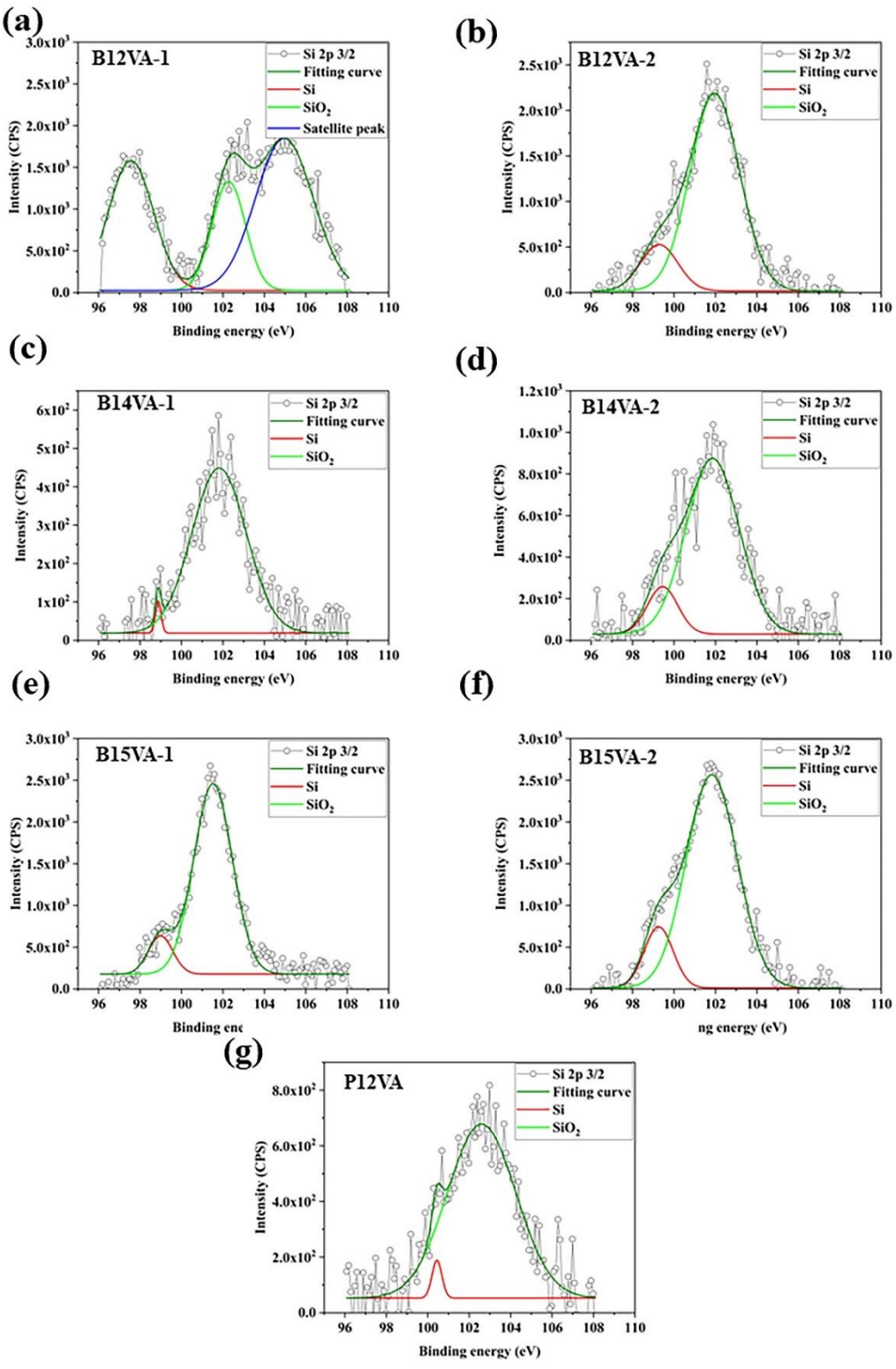


**Figure 7.19** The XPS spectrograph's peak-fitting results of Si $2p_{3/2}$ after 30 days immersion test of the austempered ( at 250°C) bainitic steels samples: (a) B12VA-1, (b) B12VA-2, (c) B14VA-1, (d) B14VA-2, (e) B14VA-1, and (f) B15VA-2 and also, pearlitic steel (at 550°C): (g) P15VA in aqueous 3.5% NaCl solution.

Blocky RA content decreases with rise in the Aus. time resulting in fewer sites of galvanic cell corrosion exists, due to which uniform corrosion occurs and leads to the development of a dense, non-porous and thin passive film on the metal surface. XPS survey spectra confirms that the peak intensity of oxide and hydroxide of the corrosion-resistant elements are higher than the less austempered bainitic steel and the pearlitic steel. At the onset of corrosion, the oxide coating initially comprises of $Fe_2O_3$ and a thin film of FeOOH. With increasing $O_2$ exposure, $Fe_3O_4$ and FeOOH continue to develop until the saturation of oxide growth is detected [205-207]. Sample B15VA-1, B15VA-2 and P15VA contain 0.43% Ni (mass%) and therefore in the XPS spectra, peaks of oxides and hydroxide of Ni are present in these samples but absent in other samples. XPS spectra of $Mo_{3d}$ are present only in the B12VA-2, B15VA-1 and B15VA-2 samples. Also, $Cr_{2p}$ peaks are observed in B12VA-1, B12VA-2, B15VA-1 and B15VA-2 samples. The presence of oxides and hydroxides of the Ni, Mo and Cr peaks makes B15VA-2 more corrosion-resistant than others.

### 7.3.3 Corrosion Product Morphology After Electrochemical and Immersion Tests

The morphologies of the corrosion products in bainitic steel samples with higher amount of RA reveals the presence of a uniform corrosion layer with the localized marginal dissolution of blocky RA along with cotton ball-like corrosion products. Kazum et al. have studied the selective marginal dissolution of RA due to the localized galvanic effect between bainite and RA [124]. Bainitic steel samples with a lesser volume fraction of RA display a uniform compact and nonporous passive corrosion layer resulting from the existence of $Fe_3O_4$ [208]. B15VA-2 and B12VA-2 samples reveal better corrosion resistance, as evident from the electrochemical test. In the polymerization of $M(O,OH)_6$, the presence of Cr and Ni ions enhances the formation of heterogeneous nucleation sites, which helps in the formation of passive protective layer [209].

Pearlitic steel samples reveal a uniform corrosion layer with some cracks in the passive layer and evidence of some pits and cotton ball-like corrosion products. Guo et al. [106] found that pearlite causes the formation of stress in the corrosion products and the possible cracking that might result from the volume expansion. The greater quantity and discontinuous distribution of pearlite induce flaws and accelerate the corrosion process. The inter-lamellar spacing of sample P15VA is lesser than P12VA and P14VA, due to which P15VA reveals better corrosion resistance than other pearlitic steels. The finer pearlite may contribute to homogeneity in the distribution of stress in the corrosion product, resulting in enhanced corrosion resistance [105].

SEM EDS of the bainitic steel samples reveals the presence of peaks of Cr, Co, Ni, Si, Mn, Al, Mo as a corrosion resistant oxide layer but reduced peak intensity of these elements are present in pearlitic steel samples.

### 7.3.4 Corrosion Mechanism

Figures 7.20(a-c) reveal the corrosion mechanism of pearlitic and bainitic steels in an aqueous 3.5% NaCl solution. Lamellar colonies of cementite and ferrite are revealed in Figure 7.20(a), in which stage1 shows that the micro level galvanic pair exists among cementite and ferrite where cementite and ferrite behave as cathode and anode, respectively in an aqueous 3.5% NaCl solution.

anodic reaction: $Fe \longrightarrow Fe^{2+} + 2e^-$

cathodic reaction: $O_2 + 4H_2O + 4e^- \longrightarrow 4OH^-$

The above reaction continues in stage 2, and greater oxidation of ferrite, and little dissolution of cementite occur.

$Fe^{2+} + OH^- = Fe(OH)_2$

In stage 3 reaction continues and more ferrite dissolves as compared to cementite and oxidation and reduction of other alloying elements occur. The formation of oxides and hydroxides of alloying elements like Cr, Ni, Co, Mo, Al, Si, and Mn resulted in the creation of a passive film, however the passive layer is broken by the presence of stress and metal substrate is exposed to NaCl solution and further corrosion occurs.

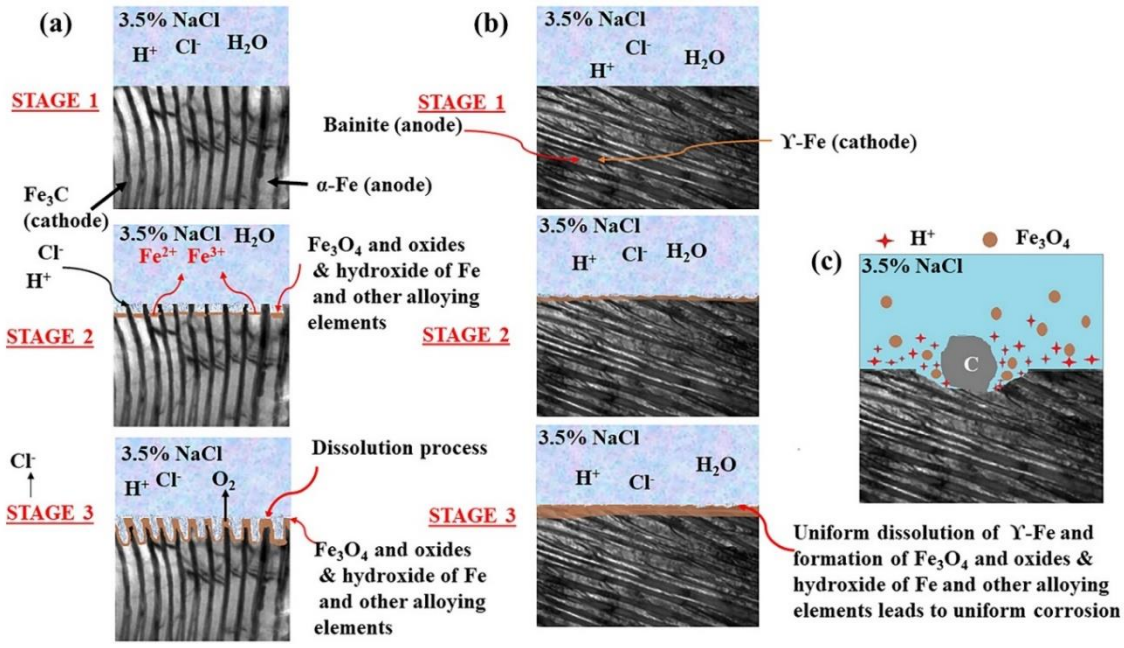


**Figure 7.20** The proposed corrosion mechanism for (a) pearlitic steel, (b) bainitic steel and (c) steel with high carbon.

In carbide-free NSB steel, finely dispersed blocky RA acts as a cathode and bainite acts as an anode in an aqueous 3.5% NaCl solution. A micro-level galvanic couple exists between RA and bainite in stage 1 (Figure 7.20(b)). The existence of fewer micro galvanic cells as well as a smaller proportion of RA led to the minimum dissolution of bainite. A similar reaction occurs in bainitic steel also, which creates a compact, uniform and non-porous thin passive layer of oxides and hydroxides of corrosion-resistant elements. This makes bainitic steel superior corrosion resistant to pearlitic steel. Figure 7.20(c) shows the corrosion mechanism for high carbon-containing steel. The presence

of carbon up to 0.23% (mass%) led to the accelerated anodic dissolution of iron, but a rise in carbon content prevents corrosion and increases magnetite production [192, 210], which restricts the exchange of ions between the solution and the metal substrate, hence enhancing the corrosion resistance of high-carbon steel. Figures 7.21(a-b) depict the cross-sectional microstructure of corroded P15VA and B15VA-2 samples, respectively. Severe pitting (22 µm) and cracks in the passive layer were observed in the pearlitic steel samples (Figure 7.21(a)) due the presence of higher number of Galvanic couples. On the other hand, uniform corrosion layer with comparatively small size pitting is recorded in bainitic steel sample (B15VA-2) (Figure 7.21(b)).

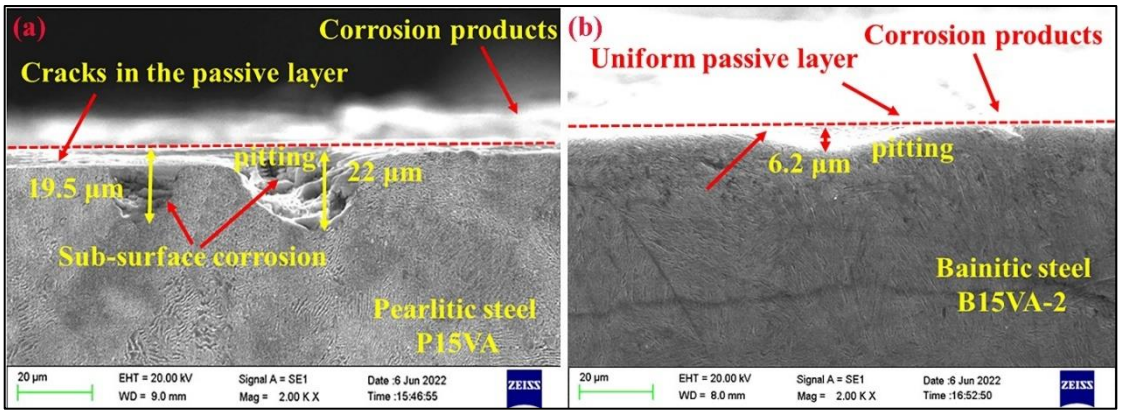


**Figure 7.21** Cross-sectional microstructure of corroded samples by secondary electron imaging in SEM (a) pearlitic steel, P15VA and (b) bainitic steel, B15VA-2.

## 7.4 CONCLUSIONS

Major conclusions drawn from the corrosion investigation are addressed below.

1. Electrochemical (EIS and potentiodynamic test) corrosion and immersion tests (30 days) confirm that a reduction in blocky austenite reduces Galvanic cell formation, which reduces the rate of corrosion.
2. However, the uniform distribution of ferrite and cementite in pearlite of patented steels form micro-level galvanic couples and promotes severe localized corrosion attacks due to the presence of stress in the corrosion layer. Therefore, corrosion

resistance of bainitic steels B12VA-2, B14VA-2 and B15VA-2 is higher than that of respective pearlitic steels P12VA, P14VA and P15VA.

3. Even though corrosion of bainitic and pearlitic steels is initiated with production of FeOOH, higher carbon content promotes the formation of a compact layer of Fe3O4. As a result, B12VA-2 shows higher corrosion resistance than B14VA-2 and P12VA also displays higher resistance than that P14VA.
4. Ni forms passive oxides of NiO in B15VA-1, B15VA-2 and P15VA, which improves corrosion resistance. Therefore, B15VA-2 is the best corrosion resistant among bainitic alloys. P15VA is the most corrosion-resistant among three pearlitic alloys. Bainitic steel shows higher corrosion resistance than pearlitic steel of same composition. B15VA-2 sample depicts an 85% lesser corrosion rate than that of the P15VA sample.